Proofs of Statements and Supplemental Experiments

In this e-companion, we provide the proofs of all statements (theorems and lemmas), and present supplemental experiments that support the robustness of the results in Section 6.2.

EC.1. Proof of Theorems and Lemmas

Proof of Lemma 1. The equilibrium state pmf is unique because the state space, $\mathbb{S}$, is finite, and the continuous-time Markov chain under study is irreducible, positive recurrent and non-null. It follows that the solution π of (4) is unique and constitutes the equilibrium state pmf.

The second part of this lemma follows, since for any given λ, μ and ν, the transition rate matrix remains unchanged because $\mathbb{S}$ is determined by S and A only, regardless of the values of G and H, as long as their sum is fixed at A. □

Proof of Theorem 1. By Lemma 1, there exists a unique equilibrium pmf for the balance equation (5). We show that any function of the form

$$\psi_B(n,k,j) = \frac{B}{\lambda^n \times \mu^k k! \times \nu^j j!}, \quad \forall (n,k,j) \in \mathbb{S}, B > 0 \tag{EC.1}$$

satisfies the balance equations of Eq. (5) by proving the validity of the following partial balance equations: (a) = (f), (b) = (d) and (c) = (e). To this end, note first the following boundary cases: when $(n,k,j) = (S,0,0)$ or $(n,k,j) = (0,S,0)$, then both (a) and (f) vanish; when $(n,k,j) = (0,S,0)$ or $(n,k,j) = (0,0,S)$, then both (b) and (d) vanish; and when $(n,k,j) = (S,0,0)$ or $(n,k,j) = (0,0,S)$, then both (c) and (e) vanish. Otherwise, the requisite equation is readily seen to hold by substituting Eq. (EC.1) into it. It follows that Eq. (6) is the unique probabilistic solution of the balance equations (5), with B^* being the normalization constant. □

Proof of Lemma 2. Since by Lemma 1, $\{(I(t), C(t), R(t)) : t \geq 0\}$ is a discrete-state, continuous-time Markov chain which is irreducible and positive recurrent and non-null, it follows that so is its jump chain.

Figure EC.1 depicts a graph fragment showing all types of feasible transitions in the cash conversion process $\{(I(t), C(t), R(t)) : t \geq 0\}$, focusing on a generic state (n,k,j). Note

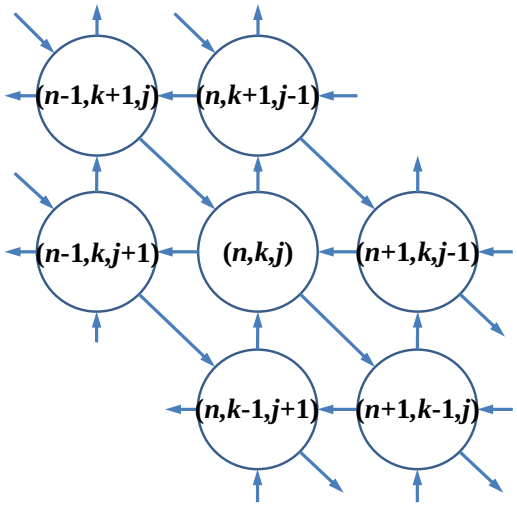

Figure EC.1 State Transition Diagram to/from State (n,k,j)

that if (n,k,j) is a boundary state (e.g., a state with $n=0$ or $k=0$ or $j=0$), then some transitions may be infeasible, but this does not invalidate the discussion to follow.

From Figure EC.1, there are exactly three types of state transitions:

- Transitions in a westerly direction are due to a demand arrival at a non-empty inventory, resulting in j increased by 1 and n decreased by 1.
- Transitions in a northerly direction are due to a payment for a receivable, resulting in k increased by 1 and j decreased by 1.
- Transitions in a southeasterly direction are due to a replenishment, resulting in n increased by 1 and k decreased by 1.

Consider any path traversed via state transitions starting in any state (n,k,j) and terminating in the same state. Suppose that the path included exactly $d \geq 1$ transitions in a northerly direction. Then Figure EC.1 shows that to return to state(n,k,j), the path must include also exactly d transitions in a southeasterly direction and exactly d transitions in a westerly direction, for a total of $3d$ transitions. A similar argument holds for paths which include d transitions in a southeasterly direction and westerly direction, implying that state (n,k,j) has period 3. Since the periodicity is a class property, we conclude that $\{(I(t),C(t),R(t)) : t \geq 0\}$ is periodic with period 3. $\square$

Proof of Theorem 2. The existence and uniqueness of π and π^J follow from Lemma 2. The equilibrium state pmf vectors π and π^J are related by (Kelly 1979, pp. 4–5)

$$\pi^J(s) = \frac{\pi(s)q(s)}{\sum_{u\in\mathbb{S}} \pi(u)q(u)}, \quad s \in \mathbb{S}. \tag{EC.2}$$

Eq. (8) follows readily from Eq. (EC.2). Furthermore, from Theorem 3.10 in Çinlar (1975), for an irreducible positive recurrent non-null Markov chain, π^J is also the limiting pmf vector satisfying for any initial row probability vector ψ,

$$\pi^J = \begin{cases} \lim\limits_{n\to\infty} \psi \mathbf{P}^n & \{M^J(t) : t \geq 0\} \text{ is aperiodic} \\ \psi \frac{\sum_{k=1}^{K} \mathbf{P}^k}{K} \lim\limits_{n\to\infty} \left(\mathbf{P}^K\right)^n & \{M^J(t) : t \geq 0\} \text{ is periodic with period } K \end{cases} \tag{EC.3}$$

where ψ is any probability vector over the state space $\mathbb{S}$. Thus, Eq. (9) follows from Eq. (EC.3) as a special case for period $K = 3$. □

Proof of Lemma 3. For $s = (n, k, j)$ satisfying $1 \leq n \leq S$ and $0 \leq k \leq G + H - n$, one has $\Theta(\cdot, s) = \{(n-1, k+1, j)\}$. The corresponding transition rate is $q\left((n-1, k+1, j), (n, k, j)\right) = L_{n-1,k+1}\mu$. Thus,

$$\sum_{u\in\Theta(\cdot,s)} \pi(u)\, q(u, s) = \pi(n-1, k+1, j)\, L_{n-1,k+1}\, \mu. \tag{EC.4}$$

Similarly, for $v = (n'+1, k'-1, j')$ where $0 \leq n' \leq S-1$ and $1 \leq k' \leq G+H-n'$,

$$\sum_{(u,v)\in\Theta} \pi(u)\, q(u, v) = \sum_{u\in\Theta(\cdot,v)} \pi(n', k', j')\, L_{n',k'}\, \mu = \sum_{n'=0}^{S-1} \sum_{k'=1}^{G+H-n'} \pi(n', k', j')\, L_{n',k'}\, \mu. \tag{EC.5}$$

Eq. (13) follows readily by substituting Eqs. (EC.4) and (EC.5) into Eq. (12). □

Proof of Lemma 4. Given that a PEMU transitions from the treasury to the inventory and "sees" there exactly n PEMUs (including itself) just after transition, then it is the sum of n independent exponential random variables, each with rate λ. Thus, the corresponding conditional sojourn time density is Erlang with rate parameter λ and shape parameter n, whence

$$f_{T_I|I(\tau_i^\Theta)}(t|n) = \frac{\lambda^n t^{n-1} e^{-\lambda t}}{(n-1)!}. \tag{EC.6}$$

It follows that

$$f_{T_I}(t) = \sum_{n=1}^{S} \pi_I^\Theta(n) f_{T_I|I(\tau_i^\Theta)}(t|n) \tag{EC.7}$$

where $\pi_I^{\Theta}(n)$ is the marginal pmf vector of π^{Θ} of the embedded inventory size given by Eq. (15). Eq. (15) follows by substituting Eq. (EC.6) into Eq. (EC.7). $\square$

Proof of Theorem 3. We first obtain the equilibrium density function $f_{T_C}(t)$ of random variable T_C. From Eq. (10) and by the independence of T_I and T_R, the density of their sum is the convolution of the respective densities. Using the f_{T_I} and f_{T_R} representations in Eqs. (15) and (16), respectively, we have

$$\begin{aligned} f_{T_C}(t) &= \int_0^t f_{T_I}(x) f_{T_R}(t-x)dx \\ &= \int_0^t \sum_{n=1}^{S} \pi_I^{\Theta}(n) \frac{\lambda^n x^{n-1} e^{-\lambda x}}{(n-1)!} \nu e^{-\nu(t-x)} dx \\ &= \sum_{n=1}^{S} \pi_I^{\Theta}(n) \frac{\lambda^n \nu e^{-\nu t}}{(n-1)!} \int_0^t x^{n-1} e^{(\nu-\lambda)x} dx \end{aligned} \tag{EC.8}$$

Now, let $a_m(t) = \int_0^t x^m e^{(\nu-\lambda)x} dx, m \geq 0$, denote the integral on the extreme right-hand side of Eq. (EC.8). Then for $m = 0$,

$$a_0(t) = \int_0^t e^{(\nu-\lambda)x} dx = \frac{e^{(\nu-\lambda)t}}{\nu-\lambda} - \frac{1}{\nu-\lambda} \tag{EC.9}$$

and for $m \geq 1$, integration by parts yields the recursive relation

$$\begin{aligned} a_m(t) &= \frac{1}{\nu-\lambda} \int_0^t x^m \left(e^{(\nu-\lambda)x}\right)' dx \\ &= \frac{1}{\nu-\lambda} \left[x^m e^{(\nu-\lambda)x} \Big|_0^t - \int_0^t (x^m)' e^{(\nu-\lambda)x} dx \right] \\ &= \frac{1}{\nu-\lambda} \left[t^m e^{(\nu-\lambda)t} - m \int_0^t x^{m-1} e^{(\nu-\lambda)x} dx \right] \\ &= \frac{e^{(\nu-\lambda)t}}{\nu-\lambda} t^m - \frac{m}{\nu-\lambda} a_{m-1}(t) \end{aligned}$$

We next prove by induction the relation

$$a_m(t) = -e^{(\nu-\lambda)t} \sum_{i=0}^{m} \frac{1}{(\lambda-\nu)^{i+1}} t^{m-i} \frac{m!}{(m-i)!} + \frac{m!}{(\lambda-\nu)^{m+1}}. \tag{EC.10}$$

For $m = 0$, Eq. (EC.10) is readily seen to reduce to Eq. (EC.9), thereby establishing the induction basis. For the induction step, assume that Eq. (EC.10) holds for $m \geq 1$, and

show that it holds for $m+1$. Accordingly,

$$\begin{aligned}
a_{m+1}(t) &= \frac{e^{(\nu-\lambda)t}}{\nu-\lambda}t^{m+1} - \frac{m+1}{\nu-\lambda}a_m(t) \\
&= \frac{e^{(\nu-\lambda)t}}{\nu-\lambda}t^{m+1} - \frac{m+1}{\nu-\lambda}\left[-e^{(\nu-\lambda)t}\sum_{i=0}^{m}\frac{1}{(\lambda-\nu)^{i+1}}t^{m-i}\frac{m!}{(m-i)!} + \frac{m!}{(\lambda-\nu)^{m+1}}\right] \\
&= -\frac{e^{(\nu-\lambda)t}}{\lambda-\nu}t^{m+1} - e^{(\nu-\lambda)t}\sum_{i=0}^{m}\frac{1}{(\lambda-\nu)^{i+2}}t^{m-i}\frac{(m+1)!}{(m-i)!} + \frac{(m+1)!}{(\lambda-\nu)^{m+2}} \\
&= -\frac{e^{(\nu-\lambda)t}}{\lambda-\nu}t^{m+1}\frac{(m+1)!}{(m+1)!} - e^{(\nu-\lambda)t}\sum_{i=1}^{m+1}\frac{1}{(\lambda-\nu)^{i+1}}t^{m+1-i}\frac{(m+1)!}{(m+1-i)!} + \frac{(m+1)!}{(\lambda-\nu)^{m+2}} \\
&= -e^{(\nu-\lambda)t}\sum_{i=0}^{m+1}\frac{1}{(\lambda-\nu)^{i+1}}t^{m+1-i}\frac{(m+1)!}{(m+1-i)!} + \frac{(m+1)!}{(\lambda-\nu)^{m+2}}
\end{aligned}$$

It shows that Eq. (EC.10) holds for $m+1$, thereby completing the induction. Now substituting Eq. (EC.10) with $m=n-1$ into the extreme right-hand side of Eq. (EC.8) yields Eq. (17).

To prove Eqs. (18) and (19) we use the facts that $f_{T_I|I(\tau_i^\Theta)}(t|n)$ is Erlang with rate parameter λ and shape parameter n, and $f_{T_R}(t)$ is exponential with rate parameter ν. Eq. (18) now follows from $E[T_C]=E[T_I]+E[T_R]$, $E[T_I|I(\tau_i^\Theta)]=\frac{n}{\lambda}$ and $E[T_R]=\frac{1}{\nu}$. Finally, noting that T_I and T_R in Eq. (10) are independent, Eq. (19) follows from $Var[T_C]=Var[T_I]+Var[T_R]$, $E[T_I^2|I(\tau_i^\Theta)=n]=\frac{n(n+1)}{\lambda^2}$ and $Var[T_R]=\frac{1}{\nu^2}$. □

Proof of Theorem 4. For a given $A=G+H$, the constraint $\frac{H}{G}\le\ell$ yields $H\le\lfloor\frac{\ell}{\ell+1}A\rfloor=\bar{H}$. For given parameters $S,A,\lambda,\mu,\nu,\omega,\eta,\gamma,\beta,\alpha$, the metric ϕ depends only on G and H (denoted as $\phi(G,H)$ for simplicity). By Lemma 1, there exists a unique equilibrium state pmf vector π, whence $\pi_I(n)$ and $\pi_C(k)$ exist, are unique, and remain invariant under any internal capital allocation of every fixed A. Thus, for $1\le H\le\bar{H}$,

$$\begin{aligned}
\Delta\phi(G,H) &= \phi(G,H)-\phi(G+1,H-1) \\
&= \left[\lambda[1-\pi_I(0)]\omega - \eta\sum_{n=1}^{S}n\pi_I(n) - \gamma G - \beta\sum_{k=0}^{H-1}(H-k)\pi_C(k) - \alpha\right] - \\
&\quad \left[\lambda[1-\pi_I(0)]\omega - \eta\sum_{n=1}^{S}n\pi_I(n) - \gamma(G+1) - \beta\sum_{k=0}^{H-2}(H-k-1)\pi_C(k) - \alpha\right] \\
&= \gamma - \beta\sum_{k=0}^{H-1}\pi_C(k)
\end{aligned} \tag{EC.11}$$

Since $\pi_C(k) > 0$ for $0 \le k \le A$, it follows that $\Delta\phi(G,H)$ is strictly decreasing in H.

With $A = G + H$ fixed, it suffices to maximize ϕ over H alone in the range $\{0,\dots,\bar{H}\}$. To this end, consider the following cases.

Case 1: $\pi_C(0) \ge \frac{\gamma}{\beta}$. Then $\Delta\phi(A-1,1) \le 0$ by Eq. (EC.11). Since $\Delta\phi(A-H,H)$ is strictly decreasing in H, we have $H^* = 0$ and $G^* = A$. This case proves the first line of Eq. (26).

Case 2: $\pi_C(0) < \frac{\gamma}{\beta}$. Then $\Delta\phi(A-1,1) > 0$. If there exists a minimal $H' \in \{2,\dots,\bar{H}\}$ such that $\Delta\phi(A-H',H') \le 0$, then $H^* = H' - 1$ since $\Delta\phi(A-H,H)$ is strictly decreasing in H. Otherwise, the maximum is obtained at the boundary $H^* = \bar{H}$. This case proves the second line of Eq. (26). □

Proof of Theorem 5. From the proof of Theorem 4, $\pi_I(n)$ and $\pi_C(k)$ remain invariant under any internal capital allocation of every fixed A. Thus, for $1 \le H \le \bar{H}$,

$$\begin{aligned}
\Delta\psi(G,H) &= \psi(G,H) - \psi(G+1,H-1) \\
&= \frac{\xi - \gamma G - \beta \sum_{k=0}^{H-1} (H-k)\pi_C(k)}{G + \sum_{k=0}^{H-1} (H-k)\pi_C(k)} - \frac{\xi - \gamma(G+1) - \beta \sum_{k=0}^{H-2} (H-k-1)\pi_C(k)}{G+1 + \sum_{k=0}^{H-2} (H-k-1)\pi_C(k)} \\
&= \frac{\xi\left[1 - \sum_{k=0}^{H-1} \pi_C(k)\right] - (\beta-\gamma)\sum_{k=0}^{H-1} (A-k)\pi_C(k)}{\left[G + \sum_{k=0}^{H-1} (H-k)\pi_C(k)\right]\left[G+1 + \sum_{k=0}^{H-2} (H-k-1)\pi_C(k)\right]}
\end{aligned} \tag{EC.12}$$

In Eq. (EC.12), since $\pi_C(k) > 0$ and $\beta \ge \gamma$, term $\xi\left[1 - \sum_{k=0}^{H-1} \pi_C(k)\right]$ decreases as H increases if $\xi > 0$, and term $(\beta-\gamma)\sum_{k=0}^{H-1} (A-k)\pi_C(k)$ increases as H increases. Therefore, if $\xi > 0$ and there exists an $H' \in \{1,\dots,A\}$ such that $\Delta\psi(A-H',H') \le 0$, then $\Delta\psi(A-H,H) \le 0$ for $H' \le H \le \bar{H}$.

To this end, we consider the following cases:

Case 1: $\xi \le 0$. Then, by Eq. (EC.12), $\Delta\psi(A-H,H) \le 0$ for any $1 \le H \le \bar{H}$, implying $H^* = 0$ and $G^* = A$.

Case 2: $\xi > 0$ and $\pi_C(0) \ge \frac{\xi}{\xi + (\beta-\gamma)A}$. Then $\Delta\psi(A-1,1) \le 0$ by Eq. (EC.12) and hence $\Delta\psi(A-H,H) \le 0$ for $1 \le H \le \bar{H}$, implying $H^* = 0$ and $G^* = A$.

Case 3: $\xi > 0$ and $\pi_C(0) < \frac{\xi}{\xi + (\beta-\gamma)A}$. Then $\Delta\psi(A-1,1) > 0$ by Eq. (EC.12). If there exists a minimal $H' \in \{2,\dots,\bar{H}\}$ such that $\Delta\psi(A-H',H') \le 0$, then $H^* = H' - 1$ since

$\Delta\psi(A-H,H) \leq 0$ for $H' \leq H \leq \bar{H}$. Otherwise, the maximum is obtained at the boundary $H^* = \bar{H}$.

Finally, the first line of Eq. (38) follows by combining Case 1 and Case 2, while the second line of Eq. (38) corresponds to Case 3. □

EC.2. Supplemental Experiments

In this section, we show that the equilibrium results obtained in Section 6.2 are quite robust in approximating the present value (which considers both the transient and equilibrium phases of the state process evolution of the cash conversion system) under reasonable conditions.

We first ran numerical experiments based on the numerical settings in Section 6.2, and observed that the transient periods are relatively short. Specifically, Figure EC.2 depicts two examples whose settings are taken from the optimal designs in Figures 4(1) and 4(2), where the parameters $\lambda = 1, \mu = \frac{1}{15}, \nu = \frac{1}{20}, G = 24, H = 24, S = 21$ were used in Figure EC.2(1), and the parameters $\lambda = 1, \mu = \frac{1}{3}, \nu = \frac{1}{5}, G = 9, H = 9, S = 8$ were used in Figure EC.2(2). Each sub-figure in Figure EC.2 depicts that the expected net profit rates (computed as the average of 100,000 random replications for successive unit time intervals) starting from four extreme initial conditions, namely, (i) all tokens are in the treasury; (ii) all tokens are in the treasury and inventory; (iii) all tokens are in the inventory and receivables; and (iv) all tokens are in the receivables. The curves show that the expected net profit rates converge quickly to steady state (which closely matches our analytical equilibrium net profit rates counterparts of Eq. (21)). Further, as expected, it appears that the system in Figure EC.2(2) converges faster than the system in Figure EC.2(1), since the receivables payment rate, ν, and the inventory replenishment rate, μ, are higher in Figure EC.2(2). We note further that, for both aforementioned systems, the slowest convergence to steady state is observed when the system starts from a high level of receivables, which would not be typical in a well-run real-life company. We mention that while the initial conditions in the examples of Figure EC.2 are on the worst-case side, their convergence to steady state is still fast.

To further show the robustness of our equilibrium results in approximating the present value of expected net profit, subject to the conditions of Section 5, we performed additional experiments on the system in Figure EC.2(1) with various experimental designs (combination of G, H and S). Since there are a large number of such designs, we chose the 15

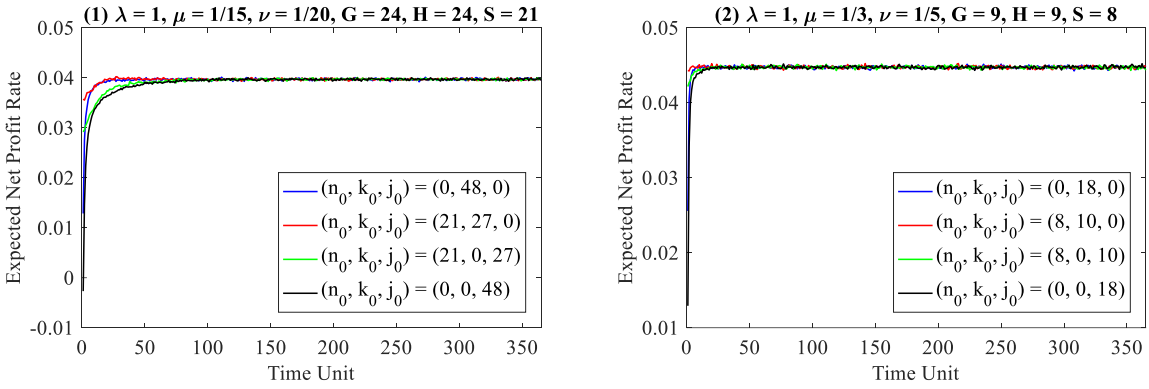

Figure EC.2 Convergence of Expected Net Profit Rate Over Time for Two Systems

designs listed in Table EC.1, where S and A range each from 10 to 50 in increments of 10 with $S \leq A = G + H$, and for each (S, A) setting, the allocation of A to G and H is computed as the optimal internal capital allocation as per Theorem 4.

Table EC.1 Experimental Designs

Design	S	$A = G + H$	G	H
1	10	10	5	5
2	10	20	10	10
3	20	20	10	10
4	10	30	15	15
5	20	30	16	14
6	30	30	16	14
7	10	40	20	20
8	20	40	21	19
9	30	40	23	17
10	40	40	23	17
11	10	50	25	25
12	20	50	25	25
13	30	50	30	20
14	40	50	32	18
15	50	50	32	18

For each design (row) in Table EC.1, we ran experiments starting the system from the extreme initial condition (state), where all PEMUs are in the treasury. Each design was simulated for 100,000 replications, and the resultant expected net profit rates over successive unit time intervals, $\phi_s(t)$, were computed. Here, t is the time interval index, ranging from 1 to the interval planning horizon index T. The system has a discount rate r, as defined in Section 5. For each design, we then compute two metrics as follows:

(1) The *simulated present value of expected net profit* over the time horizon T using the simulated realizations:

$$\sum_{t=1}^{T} e^{-rt}\phi_s(t).$$

These values serve as ground truth to which the approximation metric below will be compared to.

(2) The *equilibrium discounted net profit* over the time horizon T, computed numerically as per Eq. (22):

$$\phi_e \frac{e^{-rt_0} - e^{-rt_1}}{r} = \phi_e \frac{1 - e^{-rT}}{r},$$

where ϕ_e is the equilibrium net profit rate defined in Eq. (21). This equilibrium metric is an approximation of its simulated (non-equilibrium) counterpart above.

Figure EC.3 compares the two metrics above for each design in Table EC.1 and for various values of r and T. Specifically, the four rows in Figure EC.3 correspond to daily discount rates $r = \frac{0.05}{365}, \frac{0.1}{365}, \frac{0.2}{365}, \frac{0.3}{365}$, respectively, and the two columns in Figure EC.3 correspond to values of $T = 365, 1000$, respectively. These discount rates correspond to 5%, 10%, 20% and 30% annual discount rates, respectively, which represent a realistic range of rates in today's financial markets. The values of T are in day units, capturing reasonable time horizons of relevance to a company. In each sub-figure, the vertical axis measures the values of the two metrics above. The horizontal axis lists all design indices, but for visual clarity, the designs are sorted in ascending order of the simulated metric values.

Observing the differences between the simulated metric and its numerical equilibrium approximation, Figure EC.3 shows that for all values of r, the equilibrium approximation is very good, and hence the ranking of the designs in the order of financial goodness is identical under both metrics. Further, comparing the curves in the left column of Figure EC.3 to those in the right column, it is seen as expected that the approximations become more accurate as we increase the planning horizon T from 365 days to 1000 days. Of course, increasing the discount rate or decreasing T may adversely affect the approximation's accuracy, but for realistic discount rates and reasonably long planning horizons, the above examples support our claim that the equilibrium discounted net profit closely approximates the corresponding present value.

References

Çinlar, E. 1975. *Introduction to Stochastic Processes*. Prentice Hall.

Kelly, F.P. 1979. *Reversibility and Stochastic Networks*. Wiley.

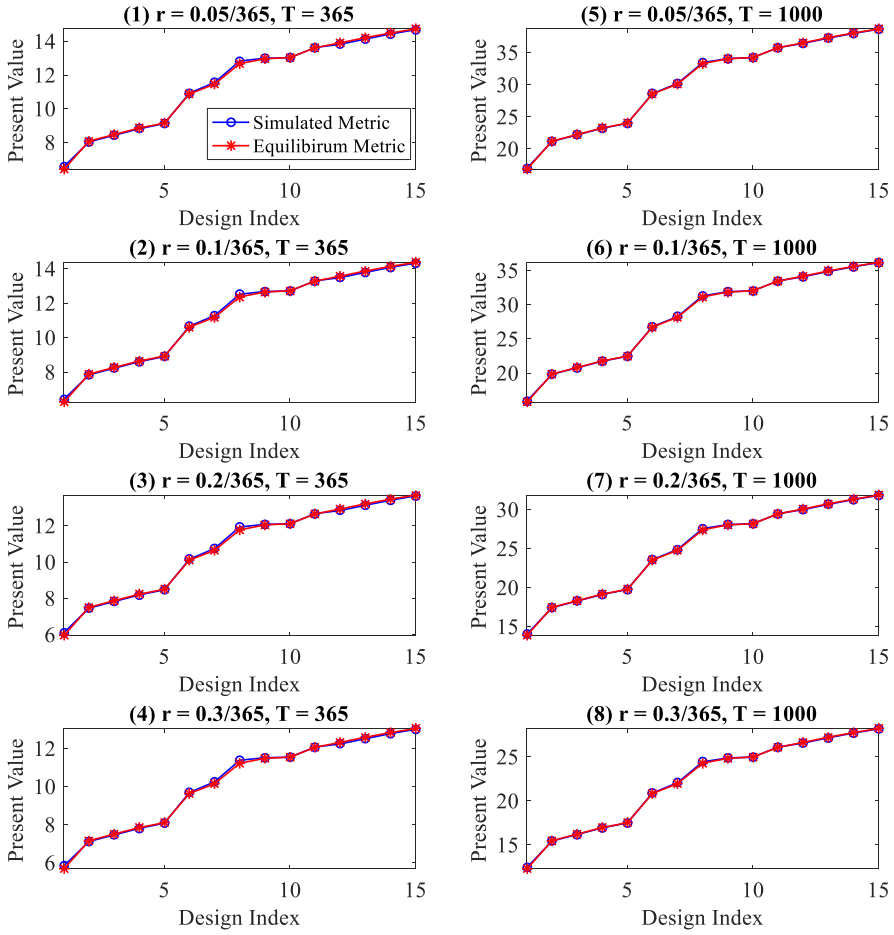

Figure EC.3 Comparison of Simulated Metrics and Their Numerical Equilibrium Approximations